Journal of Theoretical Biology 527 (2021) 110812

Contents lists available at ScienceDirect

Journal of Theoretical Biology

journal homepage: www.elsevier.com/locate/yjtbi

Global analysis of a cancer model with drug resistance due to Lamarckian induction and microvesicle transfer

Attila Dénes *, Sadegh Marzban, Gergely Röst

Bolyai Institute, University of Szeged, Szeged H-6720, Hungary

ARTICLE INFO

Article history:
Received 26 May 2020
Revised 30 April 2021
Accepted 8 June 2021
Available online 12 June 2021

2020 MSC:
34D23
92C50

Keywords:
Tumour growth model
Chemotherapy resistance
Global dynamics

ABSTRACT

Development of resistance to chemotherapy in cancer patients strongly effects the outcome of the treatment. Due to chemotherapeutic agents, resistance can emerge by Darwinian evolution. Besides this, acquired drug resistance may arise via changes in gene expression. A recent discovery in cancer research uncovered a third possibility, indicating that this phenotype conversion can occur through the transfer of microvesicles from resistant to sensitive cells, a mechanism resembling the spread of an infectious agent. We present a model describing the evolution of sensitive and resistant tumour cells considering Darwinian selection, Lamarckian induction and microvesicle transfer. We identify three threshold parameters which determine the existence and stability of the three possible equilibria. Using a simple Dulac function, we give a complete description of the dynamics of the model depending on the three threshold parameters.

We also establish an agent based model as a spatial version of the ODE model and compare the outputs of the two models. We find that although the ODE model does not provide spatial information about the structure of the tumour, it is capable to determine the outcome in terms of tumour size and distribution of cell types.

We demonstrate the possible effects of increasing drug concentration, and characterize the possible bifurcation sequences. Our results show that the presence of microvesicle transfer cannot ruin a therapy that otherwise leads to extinction, however it may doom a partially successful therapy to failure.

1. Introduction

Chemotherapy is a method for cancer treatment using anticancer drugs given as a curative agent or with the aim to prolong the patient's life and reduce the symptoms (Airley, 2009; Skeel, 2007). During chemotherapy, a single drug or a combination of drugs is usually given at intervals in pulsed doses or cycles. Cytotoxic agents damage tumour cells, which may then lead to cell death, while application of cytostatic drugs suppress tumour growth without direct cytotoxic effect. Chemotherapy resistance – a major difficulty in cancer treatment – means that a tumour previously responsive to the therapy, begins to grow as cancer cells evolve the ability to prevent the development of an effective concentration of the active agent within them. Several ways can lead to resistance of tumour cells to chemotherapy. It has been shown that tumours evolve in a similar way as Darwinian evolution acts, i.e. tumour cells are affected by selective pressure which results in the emergence of the fittest clones (Easwaran et al., 2014; Gerlinger and Swanton, 2010; Gillies et al., 2012; Li et al., 2016). In case of chemotherapy, drugs operate as selective pressure agents. Under their effect, resistant descendant cells arise in the tumour cell population. Another way of development of resistant cells is Lamarckian induction (Pisco et al., 2013), which means that a subpopulation of sensitive cells acquires resistance via changes in gene expression. A third way of appearance of resistance has recently been revealed. It is known that resistance strongly depends on intercellular communication and on tumour microenvironment. Information transfer among tumour and healthy cells affects both local and nonlocal interactions. The latter include long-range cell signalling, delivery of soluble factors and exchange of extracellular vesicles and they are responsible for the active modulation of tumour microenvironment. Microvesicles are extracellular particles released from the cell membrane transporting efflux membrane transporters, genetic information and transcription factors needed for their production in recipient cells. The important role played by microvesicles in the intercellular communication among cancer cells has been revealed by some recent

* Corresponding author.
E-mail address: denesa@math.u-szeged.hu (A. Dénes).

https://doi.org/10.1016/j.jtbi.2021.110812
0022-5193/

studies (Bebawy et al., 2009; Cesi et al., 2016; Lopes-Rodrigues et al., 2017; McNamee et al., 2018; Samuel et al., 2017; Sousa et al., 2015). The way how microvesicles emitted by more aggressive donor cells are capable to transport cellular components to less aggressive acceptor cells resembles the transmission of infectious diseases.

In Álvarez-Arenas et al. (2019), the authors provided experimental evidence from in vitro assays to show that an important exogenous source of resistance is the action of chemotherapeutic agents. This action not only affects the signalling pathways but also the interactions among cells. The authors established a mathematical kinetic transport model consisting of a system of hyperbolic partial differential equations to describe the dynamics displayed by a system of non-small cell lung carcinoma cells exhibiting a complex interplay between Darwinian selection, Lamarckian induction and the nonlocal transfer of extracellular microvesicles. Here we consider a non-spatial version of that system, that allows us to perform a comprehensive mathematical analysis of its dynamics.

To formulate our model, let us denote by $S(t)$ the number of sensitive cells at time t and let $R(t)$ stand for the number of resistant cells. We denote by $c(t)$ the drug concentration in the patient's organism at time t. Let β denote the rate of microvesicle-mediated transfer from sensitive to resistant cells and θ is the cytotoxic action induced cell mortality of sensitive cells due to drugs. The notations ρ_0 and ρ_r stand for reproduction rates of sensitive and resistant cells, respectively, here we assume $\rho_0 > \rho_r$. Parameters μ_0 and μ_r denote death rates of sensitive and resistant cells, respectively, due to apoptosis. For the tumour growth, we assume a logistic form with carrying capacity K. The letter p stands for the rate of phenotype conversion due to Lamarckian induction. The notations α and ε stand for drug uptake rate of sensitive and resistant cells, respectively, while λ_0 denotes drug removal rate. The function $I(t)$ describes time-dependent drug dosage. With these notations, our model takes the form

$$\begin{aligned} S'(t) = &\ -\beta(c(t))S(t)R(t) - \theta(c(t))S(t) + \rho_0 S(t)(K - S(t) - R(t)) - \mu_0 S(t) - p(c(t))S(t),\\ R'(t) = &\ \beta(c(t))S(t)R(t) + \rho_r R(t)(K - S(t) - R(t)) - \mu_r R(t) + p(c(t))S(t),\\ c'(t) = &\ -(\lambda_0 + \alpha S(t) + \varepsilon R(t))c(t) + I(t) \end{aligned} \tag{1}$$

In the next section we make the simplifying assumption that the drug concentration $c(t)$ is constant, and investigate the case of changing drug concentration later. This assumption transforms (1) into the system

$$\begin{aligned} S'(t) &= -\beta S(t)R(t) - \theta S(t) + \rho_0 S(t)(K - S(t) - R(t)) - \mu_0 S(t) - pS(t),\\ R'(t) &= \beta S(t)R(t) + \rho_r R(t)(K - S(t) - R(t)) - \mu_r R(t) + pS(t). \end{aligned} \tag{2}$$

In Section 2, we will give a complete characterization of the global dynamics of system (2) depending on the parameters.

2. Description of the global dynamics

2.1. Existence and local stability of equilibria

Let us define the following threshold parameters:

$$\begin{aligned} \mathscr{F}_1 &= K\rho_0 - p - \theta - \mu_0,\\ \mathscr{F}_2 &= K\rho_r - \mu_r,\\ \mathscr{F}_3 &= \mu_r(\beta + \rho_0) - (p + \theta + \mu_0 + K\beta)\rho_r. \end{aligned} \tag{3}$$

In the following, we will determine the possible equilibria of system (2) and their local stability properties depending on the parameters and describe the dynamics of (2) for all possible combinations of the signs of the above four parameters. To show which combinations of these signs cannot be realized, we prove some simple statements.

Solving the algebraic system of equations

$$\begin{aligned} -\beta SR - \theta S + \rho_0 S(K - S - R) - \mu_0 S - pS = 0,\\ \beta SR + \rho_r R(K - S - R) - \mu_r R + pS = 0, \end{aligned} \tag{4}$$

one can easily obtain the trivial equilibrium $E_0 = (0, 0)$ and the equilibrium $E_R = \left(0, K - \frac{\mu_r}{\rho_r}\right)$ where only resistant cells are present. Because of Lamarckian induction, there is no equilibrium with only sensitive cells. For any coexistence equilibrium (S^*, R^*), one obtains that the equality $S^* = (\mathscr{F}_1 - R^*(\beta + \rho_0))/\rho_0$ holds, while R^* is given as the solution of the equation $aR^2 + bR + c = 0$ with $a = \beta(\beta + \rho_0 - \rho_r), b = \mathscr{F}_3 + \beta(\mathscr{F}_2 - \mathscr{F}_1) + p(\beta + \rho_0)$ and $c = p(p + \theta + \mu_0 - K\rho_0) = -p\mathscr{F}_1$. From this, a necessary condition of a coexistence equilibrium is $\mathscr{D} := b^2 - 4ac > 0$. If, the other way around, we express R^* from the first equation, S^* is obtained as one of the solutions of the quadratic equation $\tilde{a}S^2 + \tilde{b}S + \tilde{c} = 0$ with $\tilde{a} = \beta\rho_0(\beta + \rho_0 - \rho_r) > 0, \tilde{b} = \mathscr{F}_1\beta(\rho_r - \beta - \rho_0) - \mathscr{F}_3\rho_0 - p(\beta + \rho_0)^2$ and $\tilde{c} = \mathscr{F}_1\mathscr{F}_3$. Again, the quadratic equation has real solutions if $\tilde{b}^2 - 4\tilde{a}\tilde{c} > 0$, which is equivalent to the condition $\mathscr{D} > 0$.

We prove some simple statements concerning the threshold parameters defined in (3).

Proposition 2.1. *The sensitive cells die out whenever $\mathscr{F}_1 < 0$.*

Proof. We estimate $S'(t)$ as

$$S'(t) \leqslant S(t)(K\rho_0 - p - \theta - \mu_0 - p) = \mathscr{F}_1 S(t),$$

hence, if $\mathscr{F}_1 < 0$, then $S(t) \to 0$ as $t \to \infty$.

Remark 2.2. It follows from Proposition 2.1 that no coexistence equilibrium can exist whenever $\mathscr{F}_1 < 0$.

Proposition 2.3.

i) *$\mathscr{F}_1 > 0$ and $\mathscr{F}_2 < 0$ imply $\mathscr{F}_3 > 0$.*
ii) *$\mathscr{F}_1 < 0$ and $\mathscr{F}_2 > 0$ imply $\mathscr{F}_3 < 0$.*
iii) *$\mathscr{D} < 0$ implies $\mathscr{F}_1 < 0$*

Proof. i) Suppose $\mathscr{F}_1 > 0$ and $\mathscr{F}_2 < 0$ hold but $\mathscr{F}_3 < 0$. Then we have $K\rho_0 > p + \theta + \mu_0$ and $K\rho_r < \mu_r$, hence, if $\mathscr{F}_3 < 0$ holds, then $\mu_r(\beta + \rho_0) < (p + \theta + \mu_0)\rho_r < K\rho_0\rho_r < \rho_0\mu_r$, which is a contradiction.

ii) This statement can be shown in an analogous way.

iii) In order to have $\mathscr{D} < 0$, the value $-4\beta p(\beta + \rho_0 - \rho_r)\mathscr{F}_1$ has to be positive, which can only happen is $\mathscr{F}_1 < 0$.

The following simple statement concerning the existence of a coexistence equilibrium will be useful during the complete description of the global dynamics of system (2).

Proposition 2.4. *If $\mathscr{F}_1 > 0$ and $\mathscr{F}_3 < 0$ then there is no coexistence equilibrium.*

Proof. If $\mathscr{D} < 0$ then there is no coexistence equilibrium. Let us suppose that $\mathscr{D} > 0$. From Vieta's formulas, we obtain that if $\mathscr{F}_1 > 0$ and $\mathscr{F}_3 < 0$ then the equation $aR^2 + bR + c = 0$ has exactly one positive solution as $a > 0$ and $c/a < 0$. Similarly, the equation $\tilde{a}S^2 + \tilde{b}S + \tilde{c} = 0$ also has exactly one positive solution as $\tilde{a} > 0$

and $\tilde{c}/\tilde{a} < 0$. However, we now that for any coexistence equilibrium, the equality $\rho_0 S^* + R^*(\beta + \rho_0) = \mathscr{F}_1$ holds, hence, if R_1, R_2 and S_1, S_2 are the solutions of the two quadratic equations, then, in order to fulfil the previous equality, the S and R solutions corresponding to each other must have opposite signs. From this we obtain that under the assumptions of the proposition, there cannot exist a solution of (4) with two positive coordinates.

By linearizing (2) around the equilibria E_0 and E_R, respectively, and calculating the eigenvalues of the Jacobians of the linearized systems, we obtain the following results on the local stability properties of these two equilibria.

Proposition 2.5.

i) *E_0 is locally asymptotically stable if and only if $\mathscr{F}_1 < 0$ and $\mathscr{F}_2 < 0$.*
ii) *E_R exists if and only if $\mathscr{F}_2 > 0$ and it is locally asymptotically stable if and only if $\mathscr{F}_2 > 0$ and $\mathscr{F}_3 < 0$.*

2.2. Global dynamics

In this section, we turn to the study of the global dynamics of Eq. (2). To this end, we apply the Bendixson–Dulac criterion with choosing $D(S,R) = 1/(SR)$ as a Dulac function. With this choice we obtain

$$\frac{\partial}{\partial S}\frac{-\beta SR - \theta S + \rho_0 S(K - S - R) - \mu_0 S - pS}{SR} + \frac{\partial}{\partial R} \times \frac{\beta SR + \rho_r R(K - S - R) - \mu_r R + pS}{SR} = -\frac{p + \rho_0}{R} - \frac{\rho_r}{S},$$

which is negative in the positive quadrant. Hence, using the Bendixson–Dulac theorem, we obtain that there is no periodic solution of (2). Applying the Poincaré–Bendixson theorem, it follows that all solutions tend to one of the equilibria. Based on this result and the local stability properties of the equilibria, we can give a complete characterization of the dynamics of system (2), depending on the threshold parameters $\mathscr{F}_1, \mathscr{F}_2, \mathscr{F}_3$. To state our main result describing the global dynamics of the system, we introduce the notation

$$X_S = \left\{(S,R) \in (\mathbb{R}_0^+)^2 : S = 0\right\}$$

for the extinction space of sensitive cells.

Theorem 2.6. *The global dynamics of Eq. (2) is completely determined by the threshold parameters $\mathscr{F}_1, \mathscr{F}_2, \mathscr{F}_3$ as follows.*

i) *If $\mathscr{F}_1 < 0$ and $\mathscr{F}_2 < 0$ then the only equilibrium E_0 is globally asymptotically stable.*
ii) *If $\mathscr{F}_2 > 0$ and $\mathscr{F}_3 < 0$ then E_0 is unstable. The boundary equilibrium E_R is globally asymptotically stable. There is no coexistence equilibrium in this case.*
iii) *If $\mathscr{F}_1 > 0, \mathscr{F}_2 < 0$ and $\mathscr{F}_3 > 0$ then E_0 is unstable. The coexistence equilibrium is globally asymptotically stable on $(\mathbb{R}_0^+)^2 \setminus X_S$. There is no boundary equilibrium and E_0 is globally asymptotically stable on X_S.*
iv) *If $\mathscr{F}_1 > 0, \mathscr{F}_2 > 0$ and $\mathscr{F}_3 > 0$, then E_0 and E_R are unstable and the coexistence equilibrium E_C is globally asymptotically stable on $(\mathbb{R}_0^+)^2 \setminus X_S$. The boundary equilibrium E_R is globally asymptotically stable on X_S.*

The results of Theorem 2.6 are summarized in Table 1 where all possible combinations of the signs of the threshold parameters are listed along with the description of the existence and stability of the three possible equilibria. We note that the remaining two combinations of signs cannot be realized: the combinations $\mathscr{F}_1 > 0, \mathscr{F}_2 < 0, \mathscr{F}_3 < 0$ and $\mathscr{F}_1 < 0, \mathscr{F}_2 > 0, \mathscr{F}_3 > 0$ are excluded by Proposition 2.3. The regions defined by the signs of the three threshold parameters $\mathscr{F}_1, \mathscr{F}_2, \mathscr{F}_3$ visualized in Fig. 1. The '+' and '–' characters in the regions denote the signs of the parameters $\mathscr{F}_1, \mathscr{F}_2, \mathscr{F}_3$. The figure was prepared with $\beta = 0.0957, \rho_0 = 0.1$, $K = 0.538, \mu_0 = 0.01, \mu_r = 0.0262$ and $p = 0.01$, while the parameters θ and ρ_r are varied between 0 and 0.1. Using Theorem 2.6, one can identify which of the equilibria is globally asymptotically stable on the given region. That is, E_0 is globally asymptotically stable in the lower and middle regions on the right, E_R is globally asymptotically stable in the upper right and upper left regions, while E_C is globally asymptotically stable in the middle and lower regions on the left.

3. Stochastic individual-based spatial model

In the previous section, we established an ODE model to describe tumour growth and the transfer of microvesicles between cells which are spatial problems. Our next aim is to show that the ODE model provides a good overall approximation of the spatial phenomena (of course, without giving information about the spatial structure of the tumour). Hence, in this section, we use agent-based modeling (ABM) to investigate a spatial version of Eq. (2). We will compare this spatial model with the ODE model to assess how much information that model can provide in comparison with the spatial model. In order to simulate this ABM regarding to Eq. (2), we begin by defining the assumptions of the model and then describe the important technical aspects of the model in the implementation part. The following assumptions are considered for the ABM model.

i) There are two possible states for agents: we have sensitive or resistant cells.
ii) If there is an empty space in the 8 cells Moore neighbourhood (Fig. 2(a)) of each cell, both sensitive and resistant cells divide with a probability of birth, P_b, which is equal to P_S or P_R, depending on the type of the given cell.
iii) Sensitive cells die due to apoptosis with rate μ_S, and due to drug effect with rate θ_{ABM}. Resistant cells die due to apoptosis with rate μ_R. Let P_d denote the probability of death. Hence, in sensitive cells $P_d = \mu_S + \theta_{ABM}$ and in resistant cells $P_d = \mu_R$.
iv) Phenotype conversion from sensitive to resistant cells can happen due to Lamarckian induction, the rate of which we denote by P_{ABM}. Another way of phenotype conversion is due

Table 1
Stability of equilibria depending on the threshold parameters.

$\mathscr{F}_1$	$\mathscr{F}_2$	$\mathscr{F}_3$	E_0	E_R	E_C
–	–	±	GAS	×	×
±	+	–	unstable	GAS	×
+	–	+	unstable	×	GAS
+	+	+	unstable	unstable	GAS

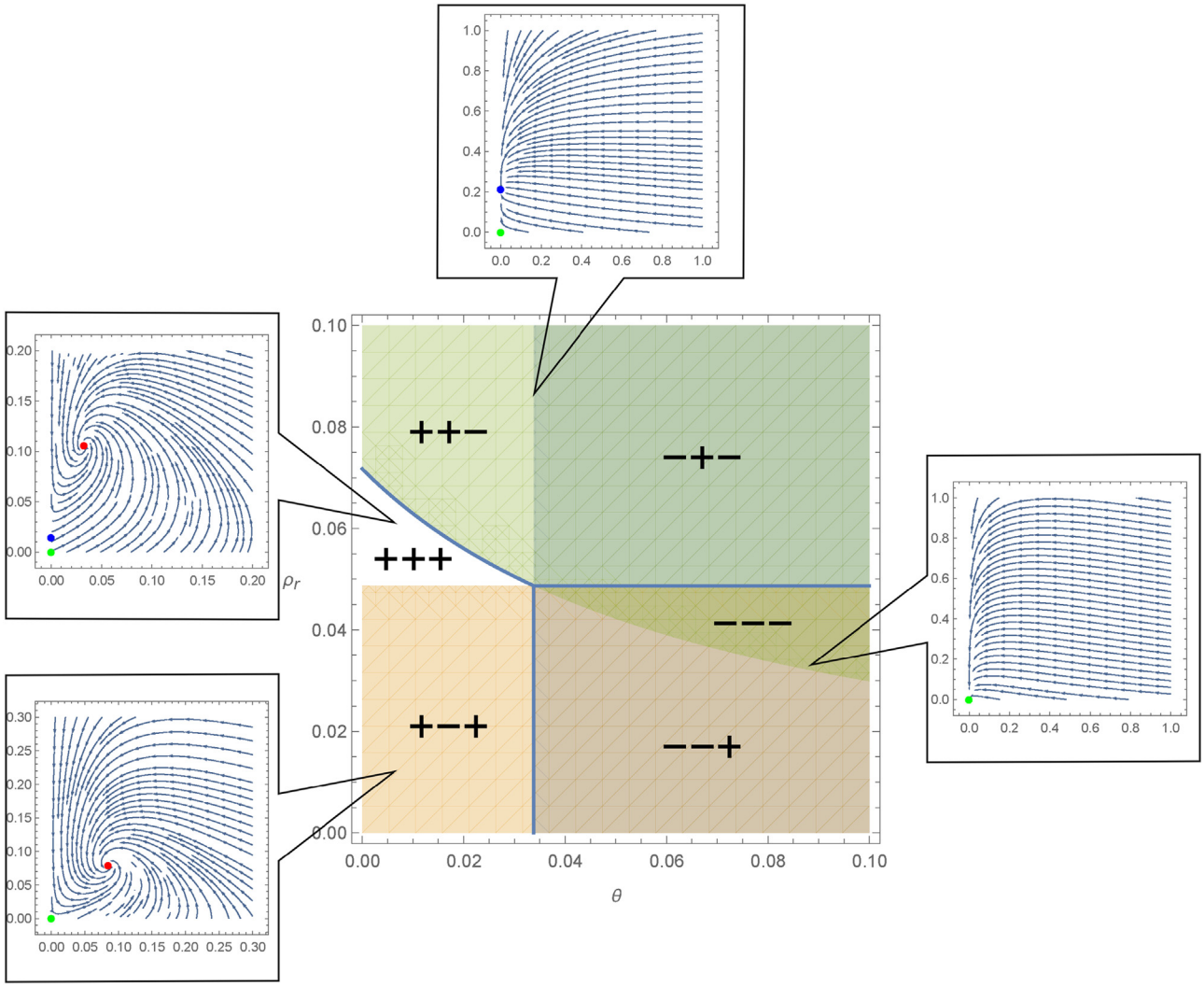

Fig. 1. Regions corresponding to the different combinations of the signs of the three threshold parameters $\mathscr{F}_1, \mathscr{F}_2, \mathscr{F}_3$.

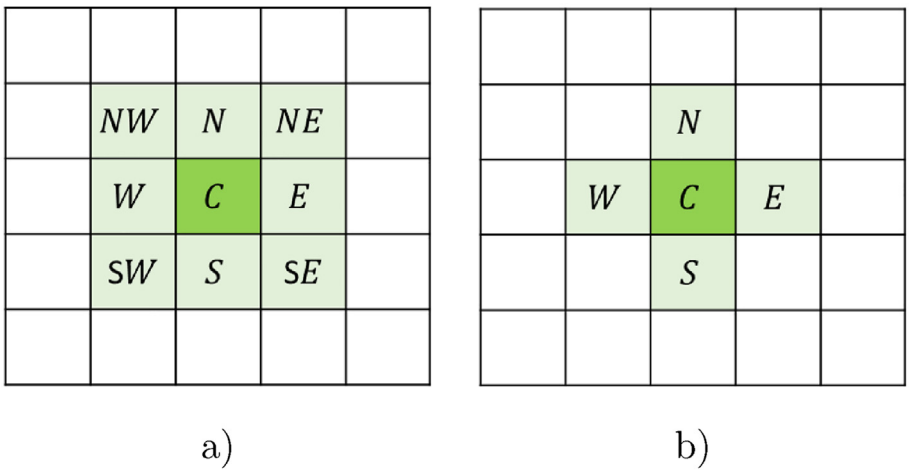

Fig. 2. a) Moore neighbourhood with radius = 1 b) von Neumann neighbourhood with radius = 1.

to the transfer of microvesicles between cells. This phenomenon is described by two parameters, namely the distance from resistant cells (if there exists resistant cell(s) in the von Neumann neighbourhood of each sensitive cell) and the rate of phenotype conversion due to microvesicles is denoted by β_{ABM} in this model.

3.1. Computational implementation

In this subsection, we describe the important aspects of the ABM implementation. Numerical simulation of the ABM is implemented by using an open-source Java library, Hybrid Automata Library (HAL) (Bravo et al., 2020). To execute the ABM model, we follow the scheme summarized in Fig. 3 as a flow diagram of our spatial model. In this model, in order to consider the division and death probability, we compare them with a random number, r_1, which is generated for each cell in population at each time-step. If $r_1 < P_d$, the cell will die, but if $P_d < r_1 < P_d + P_b$, the Moore neighbourhood of the cell will be checked and if there is an empty space in the neighbourhood, the cell will create its daughter. Moreover, to take into consideration the phenotype conversion (*sensitive* → *resistant*) due to microvesicles, we check a von Neumann neighbourhood of each sensitive cell to see the spatial effect of microvesicles. The radius of this neighbourhood can be adjusted. If there exist resistant cells in the neighbourhood, for each of them, a random number, r_2, will be generated, and then we investigate $r_2 < \beta_{ABM}$ to check if due to at least one of the resistant cells in the neighbourhood, the conversion happens. Furthermore, there is another possibility for phenotype conversion (*sensitive*

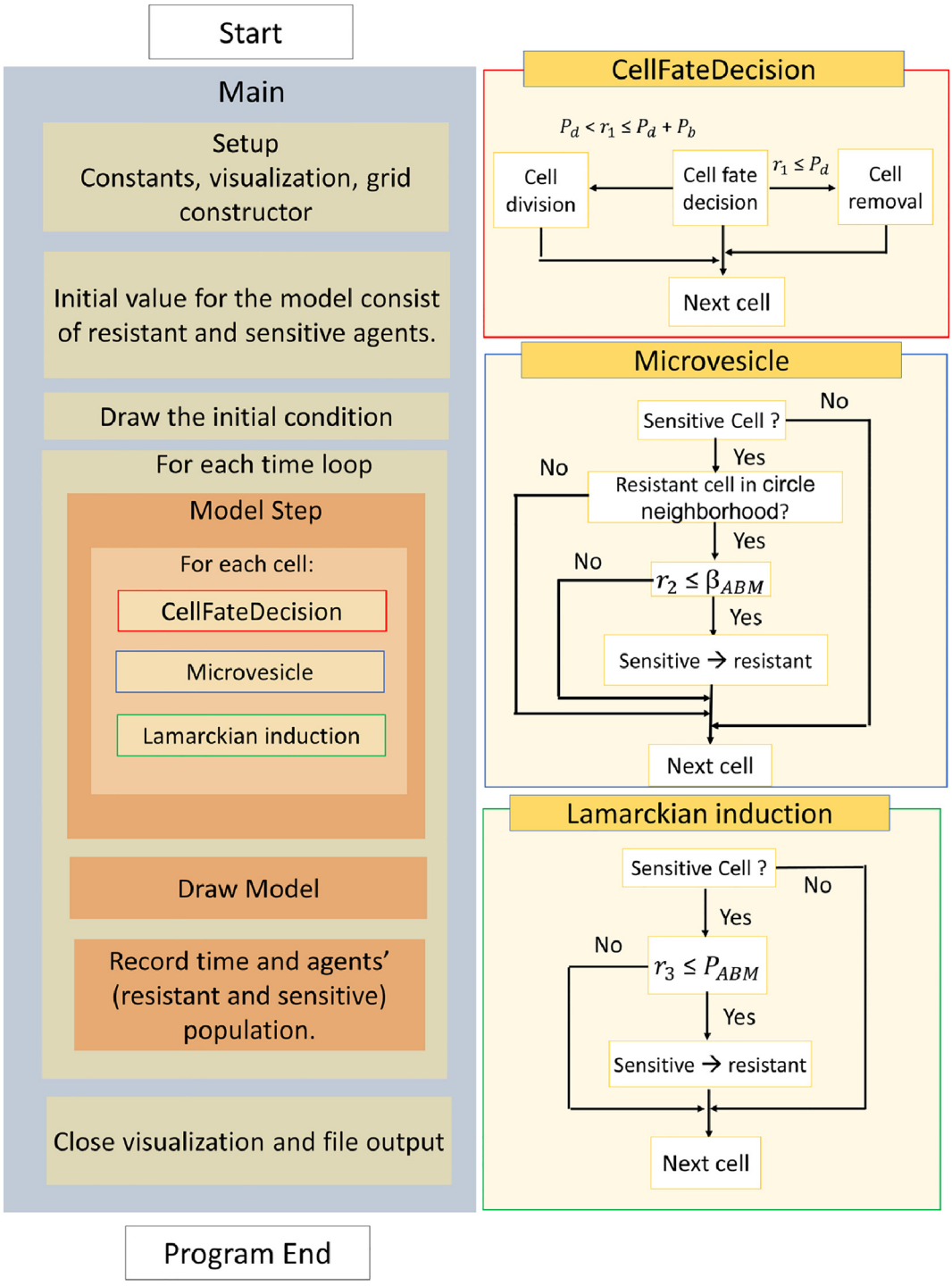

Fig. 3. ABM model flow diagram for Eq. (2).

$\rightarrow$*resistant*), due to Lamarckian induction in which case in each time loop sensitive cells convert to resistant ones with rate P_{ABM}. To take into account this conversion, we generate a random number, r_3, for each sensitive cell and if $r_3 < P_{ABM}$ this sensitive cell becomes a resistant.

4. Comparison of ABM and ODE model

4.1. Spatial model simulation

To simulate the ABM model, we start with a circle tumour (a von Neumann neighbourhood of the first tumour cell in the center of the domain) with a radius of 20 cells containing 1257 cells placed in the central domain such that 1% of them are resistant; these cells are randomly distributed among the remaining, sensitive cells. Furthermore, the domain consists of 200×200 square cells, so the total number of tumour cells cannot exceed 40000. The ABM model parameters are summarized in Table 2. Fig. 4(a) shows the simulation of the ABM model considering the values in Table 2. In this figure, blue and green cells indicate sensitive and resistant cells, respectively. We can observe the coexistence of resistant and sensitive cells in Fig. 4(a). The number of both types of cells w.r.t. time in the same scenario is shown in Fig. 5 (a). In order to study the sensitive cell mortality due to the drug, we increase θ from 0.03 to 0.12 while other parameters are fixed according to Table 2. This change leads to extinction which is demonstrated in Fig. 4(b), while the number of cells over time is plotted in Fig. 5(b). Finally, in Fig. 4(c) we depict the simulation of the ABM model with P_R increased from 0.01 to 0.1 while other parameters are fixed in Table 2. In this case, we can observe from Figs. 4(c) and 5(c) that after a while, resistant cells occupy the domain. Hence, we can observe three types of tumour destinies in the ABM model, all of which correspond to one of the scenarios described by the different regions shown in Fig. 1.

Table 2
Baseline parameters in the ABM model simulation.

Symbol	Parameter	Value
P_{ABM}	Lamarckian induction	0.01
β_{ABM}	Rate of microvesicle-mediated transfer from sensitive to resistant cells	0.1
θ_{ABM}	Cell mortality of sensitive cells due to the drug	0.03
P_R	Probability of birth in resistant cells	0.01
P_S	Probability of birth in sensitive cells	0.2
μ_R	Probability of death in resistant cells	0.03
μ_S	Probability of death in sensitive cells	0.01
R_0	Initial value of resistant cells	12
S_0	Initial value of sensitive cells	1245

4.2. Comparison between ODE and stochastic agent-based model

We established the ABM model according to the corresponding ODE model (2). To compare the simulation results obtained from the agent based model and those from the ODE model (2), in

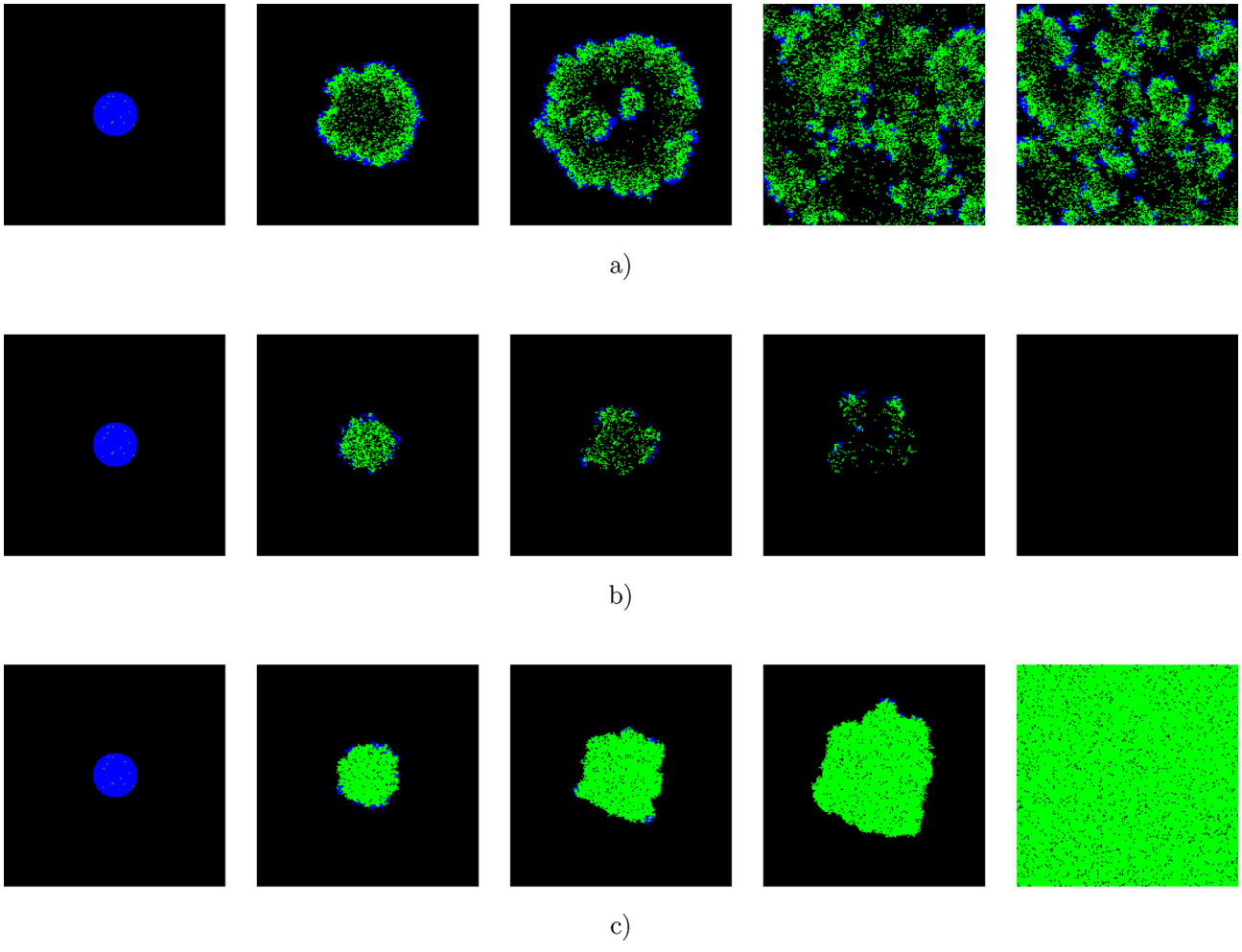

Fig. 4. ABM model simulation according to the different parameters leads to different scenarios in cells' pattern. Blue cells denote sensitive and green ones denote resistant cells. For all three simulations, all of the parameters in the ABM model are fixed as shown in Table 2. The only difference is in **b)** $\theta = 0.12$, **c)** $P_R = 0.1$.

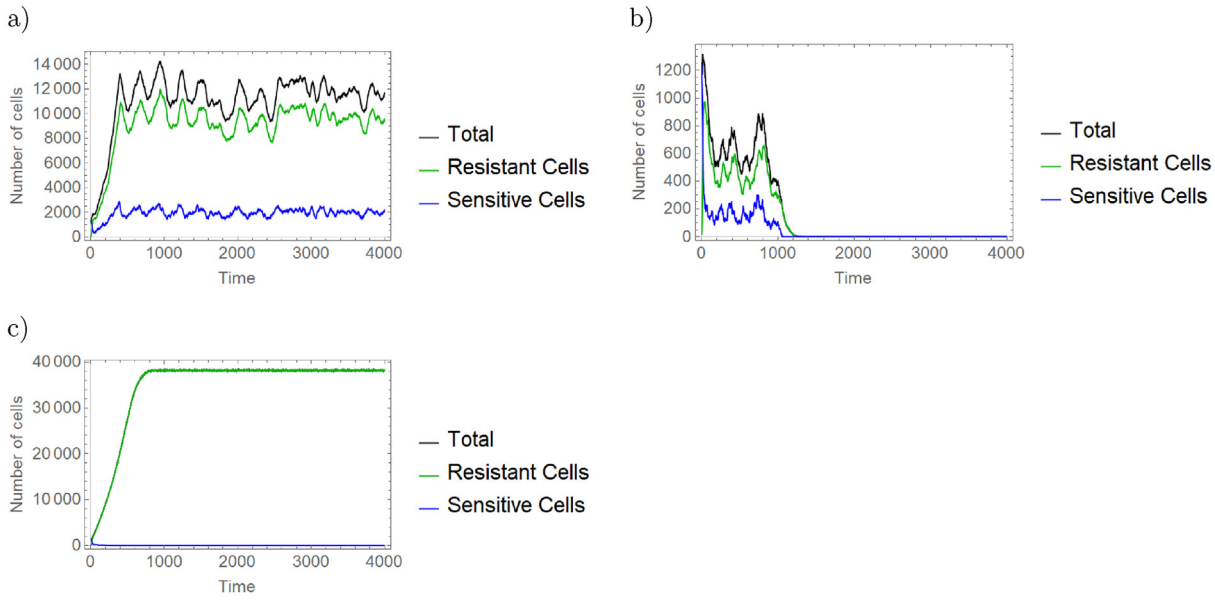

Fig. 5. The number of all tumour cells, sensitive and resistant cells in ABM model under three different parameters' values demonstrated in Fig. 4. **a)** is the simulation with parameters' values in Table 2, **b)** is the same simulation like **a** considering higher value for rate of cell mortality of sensitive cells due to the drug, $\theta = 0.12$, **c)** is also the same simulation like **a** with higher value for probability of birth in resistant cells, $P_R = 0.1$.

Fig. 8, we present solutions of (2) for various parameter sets. We note that although the same parameter values are used as for the agent based model, due to the differences in the role of the corresponding parameters of the two models, it is not possible to give a direct comparison of the results. However, the simulations can be applied to see that indeed, the outcomes of the simulations of the two models yield similar results. One can see that for both models, basically three different outcomes are possible: complete extinction of the tumour, a tumour with only resistant cells and a tumour with both sensitive and resistant cells. One can also observe that similar changes in the parameter values will yield equivalent changes in the outcomes of both models as shown by the examples presented in this section.

In spite of the equivalent qualitative results obtained from the two models, concerning the total amount of both types of cells, certainly there are quantitative differences between the two models. One of the most important of these is that in the ABM as a spatial model, we can adjust the radius of microvesicle transfer between cells, which is impossible to adjust directly in the ODE model as a non-spatial model. However, in part, it is present in the coefficient β in the ODE model as well. The main difference between the results yielded by the two models is that although we consider the effect of space in cancer cells in the ODE model, assuming parameters like β for microvesicles and K for carrying capacity, we cannot see the pattern of cell distribution in the space as we observe in the ABM model. This information about the cell pattern distribution enables us to know the growth process of the tumour, but the final outcome of tumour evolution is equivalent in both models. For instance, Fig. 6 demonstrates the difference in cells pattern due to the differences in Lamarckian induction, P_{ABM}, and microvesicles effect, β. Furthermore, Fig. 7 shows number of cells corresponding to the situations in Fig. 6. We assume all the ABM model parameters as given in Table 2, and we fix $P_S = 0.4$ for this simulation. The difference in parameters between these two simulations are in P_{ABM} and β that we assume $P_{ABM} = 0.08$ and $\beta = 0.0008$ in Fig. 6(b) which is hundred times more in P_{ABM} and this amount less in β than our assumption for these parameters ($P_{ABM} = 0.0008$ and $\beta = 0.08$) in Fig. 6(a). As seen, the cell growth procedure in these two simulations is different in the sense that the resistant cells are more randomly distributed in Fig. 6(b) than in Fig. 6(a). In contrast, as shown in Fig. 7 in both simulations, the tumour evolves into a state of coexistence of resistant and sensitive cells with more resistant cells at the end, which is a quite similar destiny. Therefore, the ABM model provides more knowledge about the transient of cells development in cancer than the ODE model while it needs more computational load.

5. Numerical simulations of the ODE model

In this section, illustrating the analytical results obtained in Section 2 concerning the ODE model (2), we perform simulations of this system to assess various phenomena regarding tumour growth. Tumour size will be given in cm^3s, accordingly, the parameter K is given in cm^3s as well. The parameters $\beta, \rho_0, \rho_r, \mu_0, \mu_r, \theta, p$ are measured in $days^{-1}$. Time is measured in days.

5.1. The effect of microvesicle transfer

An interesting question regarding the arising of chemotherapy resistance is in what extent the three ways of emergence contribute to resistance. In this subsection, we try to evaluate the effect of microvesicle transfer. Our numerical simulations suggest that microvesicle-mediated transfer might have an important role in determining the dynamics and the outcome of the treatment. It is not easy to provide a general description of this effect as it is clearly also heavily influenced by the rest of parameters, hence, here we only present one example.

In our first example, we assume time-dependent drug concentration as the drug is given to the patient in regular time intervals. The chemotherapy concentration is given by the impulsive differential equation

$$\begin{cases} c'(t) = -\lambda_0 c(t), & t \neq nT, \\ c(t^+) = c(t) + I, & t = nT, \ n = 1, 2, \dots \end{cases} \tag{5}$$

We set the parameter values as follows: $K = 6, \rho_0 = 0.3, \rho_r = 0.16, \mu_0 = 0.0024, \mu_r = 0.0531, I = 80, T = 168$. Following (Durán et al., 2016), we assume a tanh function to describe the dependence of the parameters β, p and θ on drug concentration. More precisely, these functions are assumed to have the form

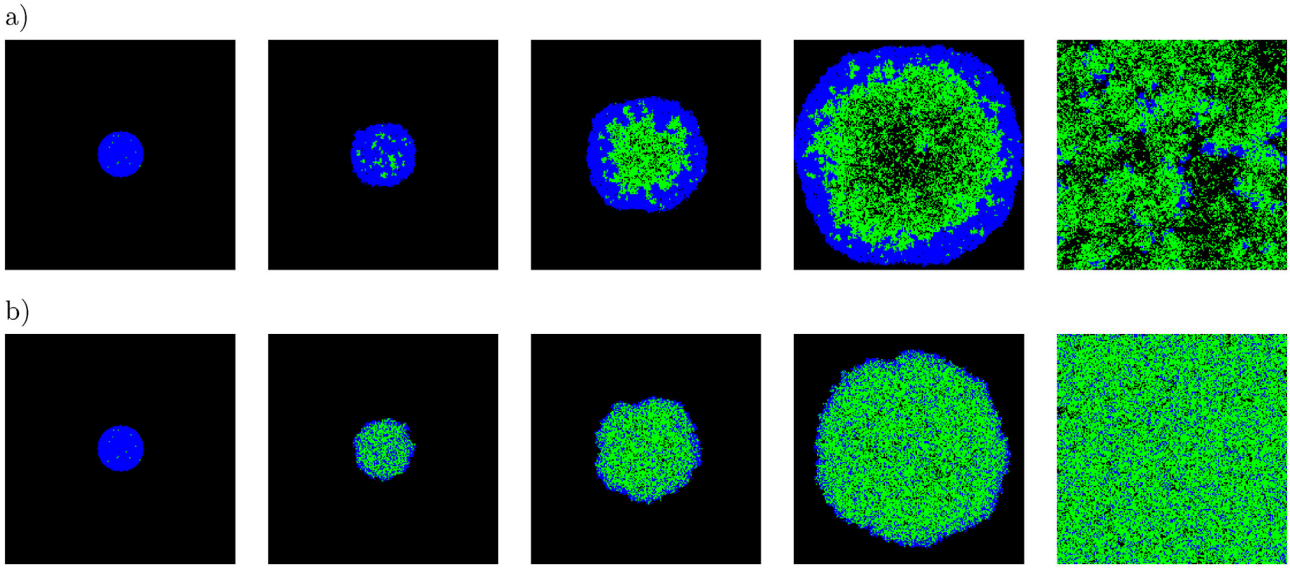

Fig. 6. Two different scenarios of cell growth considering the effect of microvesicles and Lamarckian induction. Parameters in the ABM model are as shown in Table 2 and $P_S = 0.4$. The difference between the two simulations is in **a)** $\beta = 0.08$ and $p = 0.0008$ and in **b)** $\beta = 0.0008$ and $p = 0.08$.

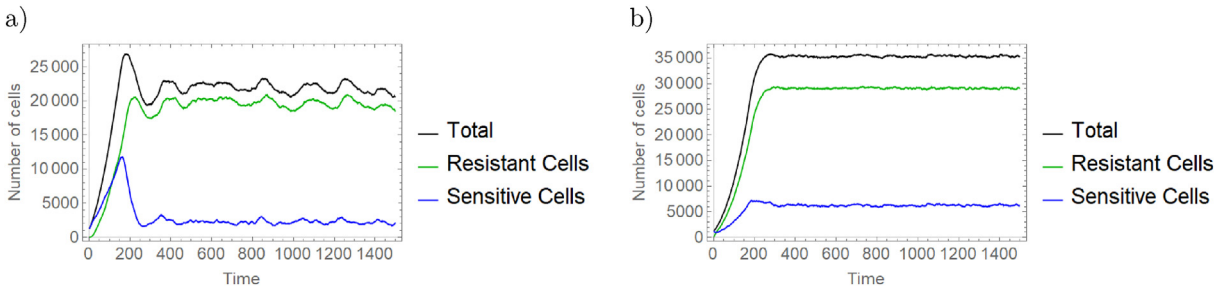

Fig. 7. The number of tumour cells including sensitive and resistant cells in ABM model under two different parameters' values demonstrated in Fig. 6. **a)**$P_S = 0.4, \beta = 0.08$ and $p = 0.0008$, **b)**$P_S = 0.4, \beta = 0.0008$ and $p = 0.08$.

$\kappa_1(1 + \kappa_2 \tanh(\kappa_3 t))$. For $p(c)$ and $\theta(c)$, the constant κ_1 takes the value 0.0066 while for $\beta(c)$ we assume $\kappa_1 = 0.0071$. For all three functions, $\kappa_2 = 5$ and $\kappa_3 = 0.02$. The parameter values ρ_0, ρ_r, K as well as the order of magnitude of the drug dosage dependent function $p(c)$ are based on Liu et al. (2018) and references therein, where the values are obtained from clinical trials. For the values of the treatment related parameters, we refer to DeConti et al. (1973) and Niiranen et al. (1992).

In Fig. 9, we show simulations with and without microvesicle-mediated transfer applying the above parameters. The situation showed in this figure might seem paradoxic at first sight, as it shows that without microvesicle transfer, the total cancer mass becomes larger, although we have excluded one way of emergence of resistance. Hence, one would expect that if there is less possibility for the arising of resistance, the chemotherapy treatment might remain more efficient. However, one can observe that in this example, reproduction rate of sensitive cells is significantly higher than that of resistant cells, while death rate is significantly higher for the latter type of cells, i.e. by ignoring this way of cells becoming resistant, we allow a larger number of much more viable sensitive cells.

5.2. The effect of drug concentration

We present numerical simulations to demonstrate what effects the change of the drug concentration c may induce. We study this through the change of the cytotoxic action induced cell mortality of sensitive cells θ and microvesicle production also depends on the concentration, assuming that these parameters are functions of the drug concentration, i.e. $\theta = \theta(c)$ and $\beta = \beta(c)$. We assume that both parameters are monotonically increasing in c, while the remaining parameters are fixed.

Example 5.1. We fix the parameter values

$$\begin{aligned} \rho_0 &= 0.0766, & \rho_r &= 0.0104, & K &= 0.752, \\ \mu_0 &= 0.0185, & \mu_r &= 0.0114, & p &= 0.0162, \end{aligned} \tag{6}$$

for which parameters the second threshold parameter has the fixed value $\mathscr{F}_2 = -0.00073 < 0$. The level curves $\mathscr{F}_1 = 0$ and $\mathscr{F}_3 = 0$ divide the positive quadrant into three regions as shown in Fig. 10. Using Theorem 2.6, we can identify the global dynamics of the system on all three regions: in the white region on the left, denoted by + – +, the coexistence equilibrium is globally asymptotically stable (except the extinction space of R, where E_0 is globally asymptotically stable), while in the two remaining regions, E_0 is globally asymptotically stable. Hence, when the curves leave the + – + region, a transcritical bifurcation occurs: the equilibrium E_C ceases to exist and E_0 becomes globally asymptotically stable.

Fig. 12(a) shows the total cancer mass, i.e. TCM $= S + R$, as a function of the drug concentration c for all five different functional forms of the increase of the concentration shown in Fig. 10.

Example 5.2. Let us now fix the parameter values as

$$\begin{aligned} \rho_0 &= 0.0766, & \rho_r &= 0.0152, & K &= 0.923, \\ \mu_0 &= 0.0185, & \mu_r &= 0.0104, & p &= 0.01. \end{aligned} \tag{7}$$

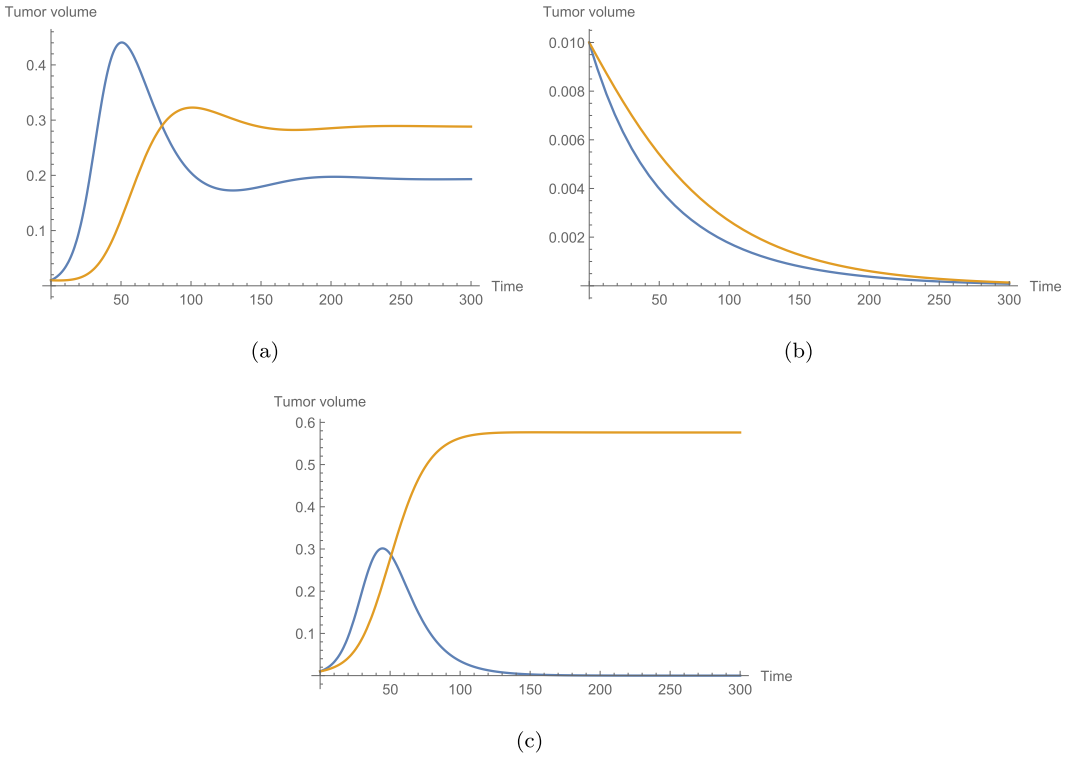

Fig. 8. The number of sensitive and resistant cells in solutions of model (2) with three different parameter sets. Figure **a)** shows solutions with parameter values in Table 2, in Figure **b)** a higher value is applied for the rate of cell mortality of sensitive cells due to the drug, $\theta = 0.17$, while in Figure **c)** we apply a higher value for the birth rate of resistant cells, $\rho_r = 0.1$. Blue curves denote sensitive, orange curves denote resistant cells.

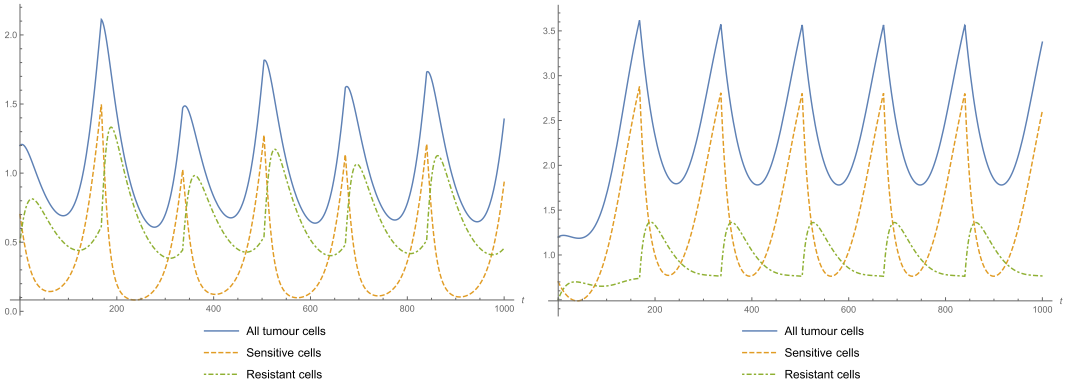

Fig. 9. Dynamics (a) with and (b) without microvesicle-mediated transfer from sensitive to resistant cells.

For these values, the threshold parameter $\mathscr{F}_2$ has the fixed value $\mathscr{F}_2 = 0.036 > 0$. For different values of the free parameters β and θ, we can experience different global dynamics depending on the sign of the remaining threshold parameters. Fig. 11 shows the plain (θ, β), divided into three regions by the level curves $\mathscr{F}_1 = 0$ and $\mathscr{F}_3 = 0$. Using Theorem 2.6, we can determine which of the equilibria is globally asymptotically stable on that region.

Hence, one can see that E_C is globally asymptotically stable in the left white region, denoted by + + +, and E_{SR} is globally asymptotically stable in the remaining two regions. Assuming different functional forms for the dependence of β and θ on the drug concentration, we can see four possible sequences of transitions among the different regions depicted in Fig. 11. When a curve passes through the boundary of the white region, a transcritical bifurcation occurs. Upon entering the white region, the previously globally asymptotically equilibrium E_R loses its stability and the newly arising coexistence equilibrium E_C becomes globally asymptotically stable.

Similarly as in the previous example, in Fig. 12(b) we depict the total cancer mass, TCM $= S + R$, as a function of the drug concentration c for the four functional forms of the increase of the concentration shown in Fig. 11.

5.3. The effect of different chemotherapy regimens

In Figs. 14(a)–(d), we show the amount of sensitive and resistant tumour cells as a function of time with different regimens of chemotherapy for various values of the parameters. For the sake of simplicity, here we neglect the drug uptake by the tumour cells.

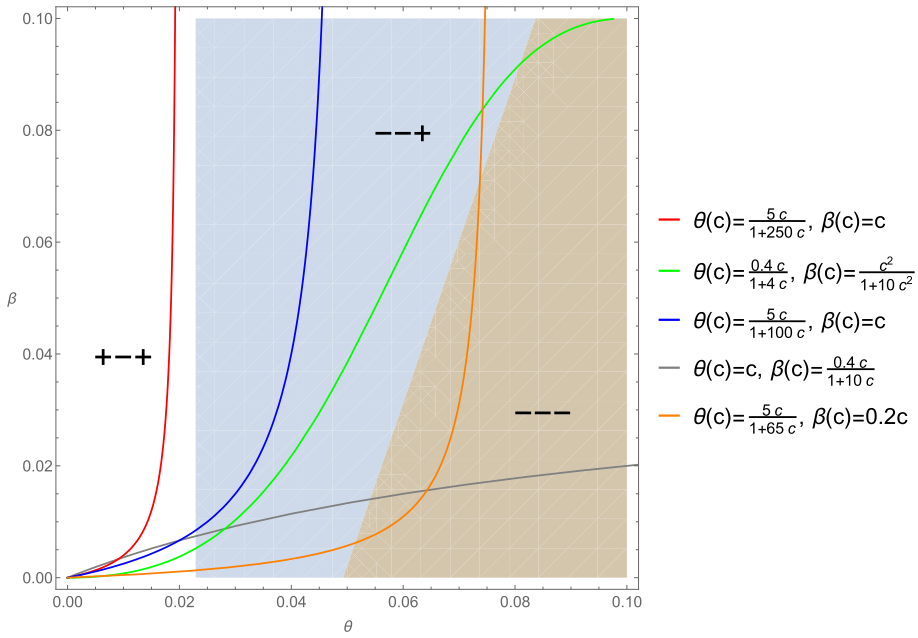

Fig. 10. Possible scenarios for the global dynamics for different drug concentrations in the (θ, β)-plain for Example 5.1. The coloured curves represent possible transitions due to change in drug concentration, assuming different functional responses to the concentration. Plus and minus signs in each region stand for the sign of the threshold parameters $\mathscr{F}_1$, $\mathscr{F}_2$ and $\mathscr{F}_3$ (see (3) and Table 1).

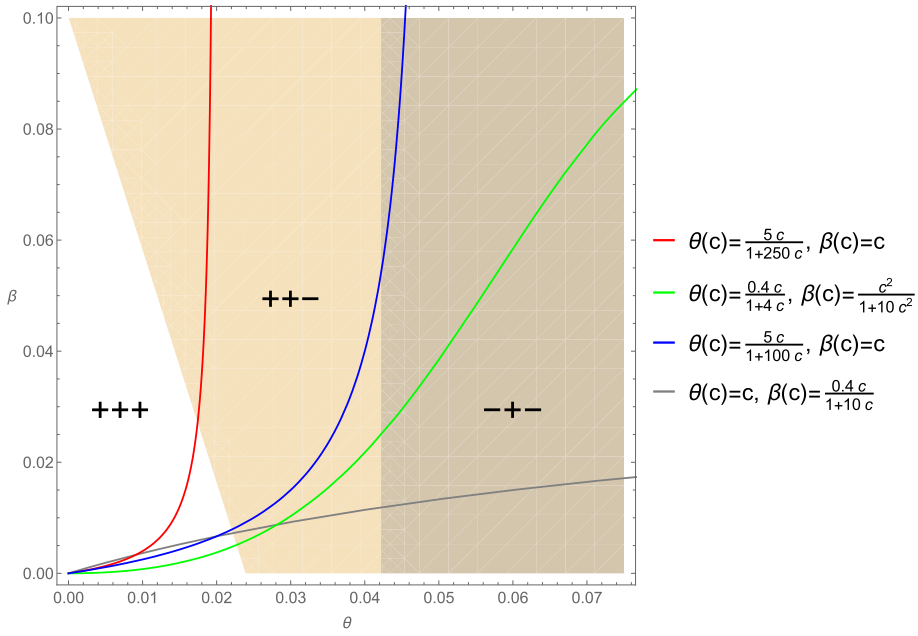

Fig. 11. Possible scenarios for the global dynamics for different drug concentrations in the (θ, β)-plain for Example 5.2. The coloured curves represent possible transitions due to change in drug concentration, assuming different functional responses to the concentration. Plus and minus signs in each region stand for the sign of the threshold parameters $\mathscr{F}_1$, $\mathscr{F}_2$ and $\mathscr{F}_3$ (see (3) and Table 1).

Again, we assume that the chemotherapy drug is given to the patients in regular time intervals as described by (5). We note that here the parameters are not biologically motivated but chosen to obtain results which illustrate several different possible outcomes. We compare three regimens which differ in the length of the time interval between receiving two doses of drug and in the amount of drug given at one treatment. The drug concentration $c(t)$ corresponding to the three different regimens of drug dosage are shown in Fig. 13.

For illustratory purposes, we assume the following functional forms for the three drug-dependent parameters:

$$\theta(c) = \frac{5c}{1+150c}, \qquad \beta(c) = \sqrt{c} \quad \text{and} \quad p(c) = 0.01c.$$

Fig. 14(a) can be interpreted as a failure of chemotherapy, as for all types of regimens, the tumour reaches a large size and all cells become resistant. Although there are slight differences between the regimens at the beginning of the therapy, finally, all three end in the same result. Figs. 14(b) and (c) show simulations where a partial success is achieved. However, in case (b), both types of cells are present, in contrary to case (c), where the sensitive cells tend to die out. In both cases, the regimen with higher dose and longer period between two treatments seems to be the most

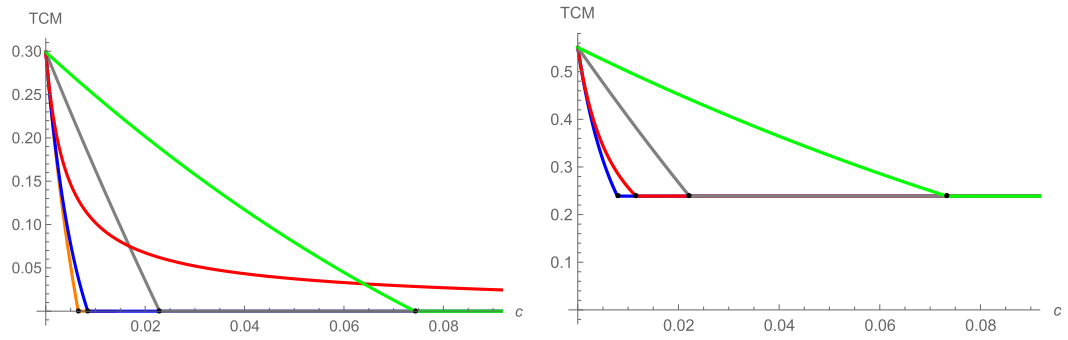

(a) $k = 0.752,\ \rho_0 = 0.0766,\ \rho_r = 0.0104,\ \mu_0 = 0.0185,\ \mu_r = 0.0114,\ p = 0.0162$ (b) $k = 0.923,\ \rho_0 = 0.0766,\ \rho_r = 0.0152,\ \mu_0 = 0.0185,\ \mu_r = 0.0104,\ p = 0.01$

Fig. 12. Total cancer mass (TCM) as a function of drug concentration c with different functional forms of $\theta(c)$ and $\beta(c)$ in the case $\mathcal{F}_2 > 0$. Functional forms are as given in Figs. 10 and 11.

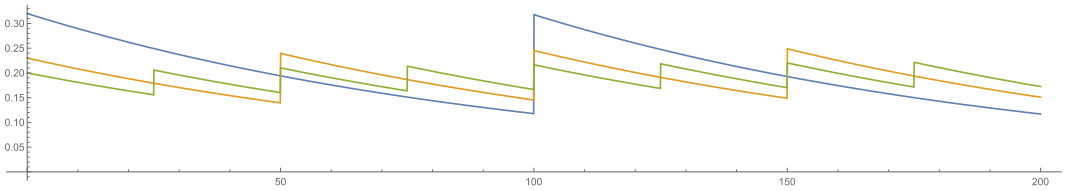

Fig. 13. Drug concentration $c(t)$ with three different regimens of drug dosage. We set $\lambda_0 = 0.01$ for all three functions. The blue curve (longest interval between two treatments and largest drug amount) was prepared with parameter $I = 0.2$, the orange one (shorter period and lower drug amount) with $I = 0.1$, the green one (shortest period and lowest drug amount) with $I = 0.05$.

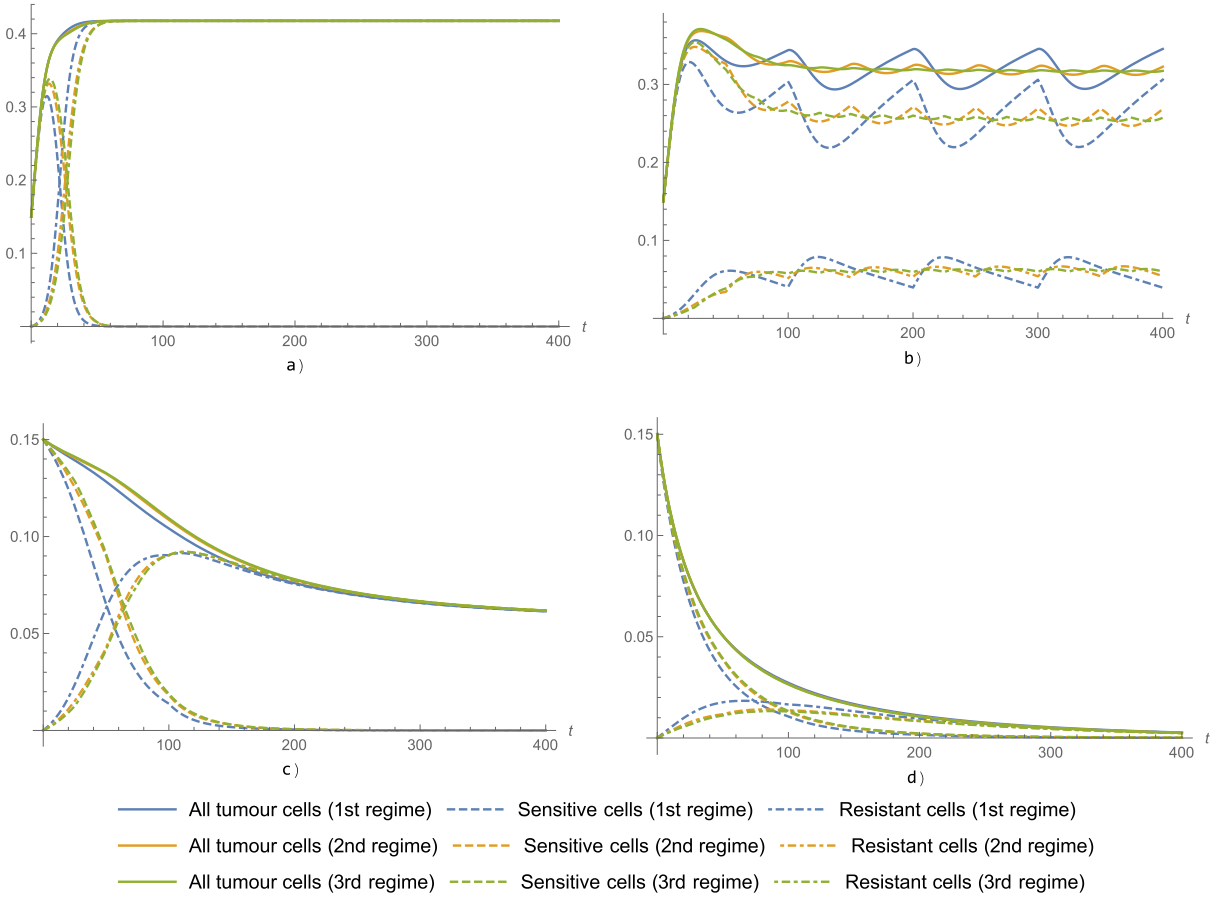

Fig. 14. The number of all tumour cells, sensitive cells and resistant cells under the three different chemotherapy regimens shown in Fig. 13 and various parameters. For all four simulations, $K = 0.5$, the rest of the parameters are as follows: a) $\rho_0 = 0.557; \rho_r = 0.281; \mu_0 = 0.0266; \mu_r = 0.0409$, b) $\rho_0 = 0.414; \rho_r = 0.154; \mu_0 = 0.0138; \mu_r = 0.15$, c) $\rho_0 = 0.157; \rho_r = 0.115; \mu_0 = 0.0257; \mu_r = 0.0509$, d) $\rho_0 = 0.166; \rho_r = 0.12; \mu_0 = 0.059; \mu_r = 0.0662$.

effective as the total number of cells is the lowest in this case. Figure (d) shows a successful treatment, where the tumour disappears for all three types of regimens.

6. Discussion

We established a mathematical model describing the evolution of tumour cells sensitive or resistant to chemotherapy. In the model, we considered three ways of emergence of chemotherapy resistance as a result of the therapeutic drug: Darwinian selection, Lamarckian induction and, based on recent discoveries, the emergence of resistance via the transfer of microvesicles from resistant to sensitive cells, which happens in a similar way as the spread of an infectious agent. Assuming constant drug concentration (a reasonably good approximation of a chemotherapy regimen with frequent treatments), we calculated the possible equilibria of the system of differential equations describing the evolution of tumour cells and determined three threshold parameters which determine the global dynamics of the system. Using the Bendixson–Dulac theorem and the Poincaré–Bendixson theorem, we gave a complete description of the global dynamics characterized by the three threshold parameters. We demonstrated the possible effects of increasing drug concentration, and characterized the possible bifurcation sequences. We showed that increasing the drug-dependent parameters β and θ might turn the coexistence equilibrium E_C unstable and, depending on the rest of the parameters, either the resistant-only equilibrium E_R or the tumour-free equilibrium E_0 becomes asymptotically stable. Another possible bifurcation is the appearance of the unstable equilibrium E_R while E_C remains asymptotically stable.

The model reveals that in the presence of Lamarckian induction, no sensitive-only equilibrium exists, while in the absence of this phenomenon, such an equilibrium exists. Moreover, in the latter case, the existence of a coexistence equilibrium is only possible if a sensitive-only equilibrium exists as well (for details, see Dénes and Röst (2020)). In other words, in case of tumour persistence, resistant cells are always present in the tumour due to Lamarckian induction.

In assessing the importance of development of resistance through microvesicle transfer, we may apply Table 1 and Figs. 10, 11 which together give us an insight into the possible scenarios that the presence of microvesicle transfer might imply. As an example, we may mention that based on these results, microvesicle transfer may turn a partially successful therapy (i.e. a decrease in the total cancer mass) to a failure (see increasing β along the red curve in Fig. 11), however, it is not able to ruin an otherwise successful therapy leading to extinction of the tumour (see increasing β along the orange curve in the right half of Fig. 10). At the same time, as suggested by the simulations in SubSection 5.1, the absence of microvesicle transfer might even lead to an increase of total cancer mass if sensitive cells are much more viable than resistant cells.

Our simple ODE model (2) certainly has its limitations. As we use ordinary differential equations, our model cannot provide information about the spatial structure of a tumour. To assess the capabilities of our model in describing tumour growth, we have also established a spatial version of the model in the form of an agent based model. Comparing the two models, we can deduce that the ODE model performs well in reproducing the possible outcomes of the tumour growth: as for total mass of the two cell types, there is no further scenario provided by the ABM than the ones experienced with the ODE model. Of course, this model will only give us information about the tumour mass and not about the spatial distribution of the two types of the tumour cells or the direction of spatial growth of the tumour. Also, the simulations suggest that the ODE model and the agent based model react in a similar way to parameter changes. Furthermore, the ODE model cannot describe the transfer of microvesicles as a spatial phenomenon in a way the ABM is capable to do so, although by modifying the parameter β in the ODE, in some extent we also consider the effect of distance between cells on the transfer of microvesicles.

In its present form, the effect of microvesicles and Lamarckian induction is described in a simple way in our model, especially in the simplified form (2). To consider these phenomena in a more realistic way can be subject of future research.

Summing up, despite its simplicity, the ordinary differential equation model is able to provide important information about the tumour growth. Although the spatial structure of the tumour is not revealed by this model, it is able to forecast key issues as tumour volume and percentage of resistant cells. The three threshold parameters can easily be calculated from the parameter values and thus provide a simple way to assess the effect of various parameter changes.

There are various directions in which the model studied here can be further developed. First of all, in this paper, we only studied analytically a version of the model with constant drug concentration. An important future work will be to study a model with time-dependent, e.g. periodic coefficients. Another possibility to make our model more realistic is to describe the effect of drug concentration on the development of resistance. For example, besides concentration, one could also consider its slope. We leave these extensions of the model as future work.

CRediT authorship contribution statement

Attila Dénes: Conceptualization, Methodology, Formal analysis, Writing - original draft, Writing - review & editing, Visualization, Investigation. **Sadegh Marzban:** Software, Investigation, Writing - review & editing, Visualization. **Gergely Röst:** Conceptualization, Methodology, Formal analysis, Investigation, Writing - review & editing, Supervision.

Declaration of Competing Interest

The authors declare that they have no known competing financial interests or personal relationships that could have appeared to influence the work reported in this paper.

Acknowledgements

The authors are grateful to the anonymous Referees for their insightful and constructive comments and suggestions which helped to improve the paper.

A. Dénes was supported by the Hungarian National Research, Development and Innovation Office grant NKFIH PD 128363 and by the János Bolyai Research Scholarship of the Hungarian Academy of Sciences. S. Marzban was supported by NKFIH KKP 129877. G. Röst was supported by EFOP-3.6.1-16-2016-00008 and NKFIH FK 124016 and 20391-3/2018/FEKUSTRAT.

References

Airley, R., 2009. Cancer Chemotherapy, Wiley-Blackwell.

Álvarez-Arenas, A. et al., 2019. Interplay of Darwinian selection, Lamarckian induction and microvesicle transfer on drug resistance in cancer. Sci. Rep. 9, Article No. 9332. doi: 10.1038/s41598-019-45863-z.

Bebawy, M. et al., 2009. Membrane microparticles mediate transfer of p-glycoprotein to drug sensitive cancer cells. Leukemia 23, 1643–1649. https://doi.org/10.1038/leu.2009.76.

Bravo, R.R. et al., 2020. Hybrid Automata Library: A flexible platform for hybrid modeling with real-time visualization. PLoS Comput. Biol. 16, (3) e1007635.

Cesi, G. et al., 2016. Transferring intercellular signals and traits between cancer cells: extracellular vesicles as "homing pigeons". Cell Commun. Signal. 14 (13), doi: 10.1186/s12964-016-0136-z.

DeConti, R.D. et al., 1973. Clinical and pharmacological studies with cis-Diamminedichloroplatinum(II), Cancer Res. 33, 1310–1315.

Dénes, A., Röst, G., 2020. Global analysis of a cancer model with drug resistance due to microvesicle transfer. In: Mondaini, R.P. (Ed.), Trends in Biomathematics: Modeling Cells, Flows, Epidemics, and the Environment. Springer, Cham, pp. 71–80. https://doi.org/10.1007/978-3-030-46306-9_5.

Durán, M.R. et al., 2016. Transfer of drug resistance characteristics between cancer cell subpopulations: a study using simple mathematical models, Bull. Math. Biol. 78, 1218–1237.

Easwaran, H., Tsai, H.-C., Baylin, S.B., 2014. Cancer epigenetics: tumour heterogeneity, plasticity of stem-like states, and drug resistance. Mol. Cell 54, 716–727. https://doi.org/10.1016/j.molcel.2014.05.015.

Gerlinger, M., Swanton, C., 2010. How Darwinian models inform therapeutic failure initiated by clonal heterogeneity in cancer medicine. Br. J. Cancer 103, 1139–1143. https://doi.org/10.1038/sj.bjc.6605912.

Gillies, R.J., Verduzco, D., Gatenby, R.A., 2012. Evolutionary dynamics of carcinogenesis and why targeted therapy does not work. Nat. Rev. Cancer 12, 487–493. https://doi.org/10.1038/nrc3298.

Li, Q. et al., 2016. Dynamics inside the cancer cell attractor reveal cell heterogeneity, limits of stability, and escape. Proc. Natl. Acad. Sci. USA 113, 2672–2677. https://doi.org/10.1073/pnas.1519210113.

Liu, X. et al., 2018. A deterministic and stochastic model for the system dynamics of tumour-immune responses to chemotherapy, Physica A 500, 162–176.

Lopes-Rodrigues, V. et al., 2017. Identification of the metabolic alterations associated with the multidrug resistant phenotype in cancer and their intercellular transfer mediated by extracellular vesicles. Sci. Rep. 7, 44541. https://doi.org/10.1038/srep44541.

McNamee, N. et al., 2018. Extracellular vesicles and anti-cancer drug resistance. BBA Rev. Cancer 1870, 123–136. https://doi.org/10.1016/j.bbcan.2018.07.003.

Niiranen, A. et al., 1992. Adjuvant chemotherapy after radical surgery for non-small-cell lung cancer: A randomized study. J. Clin. Oncol. 10, 1927–1932. https://doi.org/10.1200/JCO.1992.10.12.1927.

Pisco, A. et al., 2013. Non-Darwinian dynamics in therapy-induced cancer drug resistance. Nat. Commun. 4, 2467. https://doi.org/10.1038/ncomms3467.

Samuel, P. et al., 2017. Mechanisms of drug resistance in cancer: the role of extracellular vesicles. Proteomics 17, 1600375. https://doi.org/10.1002/pmic.201600375.

Skeel, R.T., 2007. Handbook of Cancer Chemotherapy. Lippincott Williams & Wilkins.

Sousa, D. et al., 2015. Intercellular transfer of cancer drug resistance traits by extracellular vesicles. Trends Mol. Med. 21, 595–608. https://doi.org/10.1016/j.molmed.2015.08.002.